Available online at www.sciencedirect.com
ScienceDirect
Trans. Nonferrous Met. Soc. China 30(2020) 3006−3015
Transactions of Nonferrous Metals Society of China
www.tnmsc.cn

Microstructure and high-temperature mechanical properties of near net shaped Ti−45Al−7Nb−0.3W alloy by hot isostatic pressing process

Hui-zhong LI[1,2,3], Yi-xuan CHE[1], Xiao-peng LIANG[1,2,3], Hui TAO[1], Qiang ZHANG[1], Fei-hu CHEN[1], Shuo HAN[1], Bin LIU[2]

1. School of Materials Science and Engineering, Central South University, Changsha 410083, China;
2. State Key Laboratory of Powder Metallurgy, Central South University, Changsha 410083, China;
3. Key Laboratory of Nonferrous Metal Materials Science and Engineering, Ministry of Education, Central South University, Changsha 410083, China

Received 8 January 2020; accepted 31 July 2020

Abstract: Near net shaped Ti−45Al−7Nb−0.3W alloy (at.%) parts were manufactured by hot isostatic pressing (HIP). The microstructure and high-temperature mechanical properties of the alloy were investigated by X-ray diffractometry (XRD), scanning electron microscopy (SEM) and transmission electron microscopy (TEM). The results show that at a temperature of 700 °C, the peak yield stress (YS) and ultimate tensile stress (UTS) of alloy are 534 and 575 MPa, respectively, and the alloy shows satisfactory comprehensive mechanical properties at 850 °C. The alloy exhibits superplastic characteristics at 1000 °C with an initial strain rate of 5×10^{-5} s^{-1}. When the tensile temperature is below 750 °C, the deformation mechanisms are dislocation movements and mechanical twinning. Increasing the tensile temperature above 800 °C, grain boundary sliding and grain rotation occur more frequently due to the accumulation of dislocations at grain boundary.

Key words: TiAl alloy; near net shape; powder metallurgy; high-temperature mechanical properties

1 Introduction

TiAl-based alloys are considered as promising structural materials for aerospace, automotive and energy industries because of their low density, good high-temperature strength, good creep resistance and high resistance to oxidation [1−3]. Powder metallurgy (PM), especially hot isostatic pressing (HIP) provides an alternative way to produce high quality TiAl alloys [4−6]. In recent years, HIP has been applied to manufacturing the nearly fully dense parts with the refined and homogenous microstructure [7,8], even for metal parts with high precision and complex shape [9−11].

Many researchers have studied the influence of the HIP process parameters and densification behavior of TiAl alloy. HE et al [12] studied the microstructural characteristics and densification behavior of high-Nb TiAl powder, and found that microstructure and properties of HIPed billets were influenced by the particle size of plasma rotating electrode processed powders. The microstructure of the HIPed billets produced by consolidating powder with particle size at 105−200 μm showed some primary particle boundaries and coarse lamellar structure flaws, which had apparently inherited effects on the final consolidated billet after HIP process. HABLE and MCTIERNAN [13] studied the effects of HIP temperature (between 1200 and

Foundation item: Project (51774335) supported by the National Natural Science Foundation of China; Project (2019JJ40374) supported by the Natural Science Foundation of Hunan Province, China; Project (CSUZC202004) supported by the Open Sharing Fund for the Large-scale Instruments and Equipments of Central South University, China
Corresponding author: Xiao-peng LIANG; Tel: +86-18684894344; E-mail: liangxp@csu.edu.cn; mselxp@163.com
DOI: 10.1016/S1003-6326(20)65438-3

1300 °C) on tensile properties of the Ti−46Al−2Cr−2Nb alloy, and found that the effect of HIP temperature on tensile properties is small when microstructural differences are largely eliminated. The tensile properties are more closely related to microstructure. YANG et al [14] studied the effects of heat treatment and particle size on the microstructures and tensile properties of the HIPed Ti4522XD alloy. They found that powder size and post-HIP aging had no significant influence on tensile properties, the HIPed microstructure of Ti4522XD alloy depended on the HIP temperature. There are some research reports on the mechanical properties of HIPed TiAl alloy at room temperature in Refs. [13,14], and limited investigations were conducted on the high-temperature properties of HIPed TiAl alloy. SHAGIEV et al [15] found that when the temperature was higher than 1000 °C, the HIPed Ti−47Al−3Cr alloy exhibited superplastic deformation characteristics.

The relationship among high-temperature mechanical properties, microstructure and deformation mechanisms of powder metallurgy HIPed TiAl alloys are complex [16−18]. Our previous work [19−21] focused on the hot forging and rolling process of a PM Ti−45Al−7Nb−0.3W alloy, and found that the high-temperature (above eutectoid temperature) deformation mechanisms of TiAl alloy were grain boundary sliding, mechanical twins and dynamic recrystallization.

In this work, a near net shaped Ti−45Al−7Nb−0.3W part was manufactured by HIP. The microstructure and high-temperature mechanical properties were investigated, and the deformation mechanism lower than eutectoid temperature was disscused.

2 Experimental

The Ti−45Al−7Nb−0.3W (at.%) pre-alloyed powders with particle size <100 μm were produced by plasma rotating electrode process (PREP), and the characteristics of the pre-alloyed powders have been reported in Refs. [12,19]. The near net shaped part was manufactured by HIP with powder and a mold core. The mold core model and the prepared part are shown in Fig. 1. The mold core model in Fig. 1(a) was prepared by high-purity graphite. The mold core and powder were placed in a stainless steel package and then vacuumed at 500 °C. Subsequently, the stainless steel can with powder and mold core were consolidated by HIP at 1250 °C and 150 MPa for 5 h, with a heating rate of 10 °C /min. After HIP treatment, the sample was cooled in furnace from 1250 to 100 °C in 6 h followed by air cooling. The HIPed TiAl alloy part has an oxygen content of 750×10^{-6} and a density of 99.8%. Figures 1(b) and (c) give the macrographs of the HIPed sample with and without package, respectively. By removing the extra parts and cleaning the surface of the sample, the HIPed near net shaped part is obtained (Fig. 1(d)).

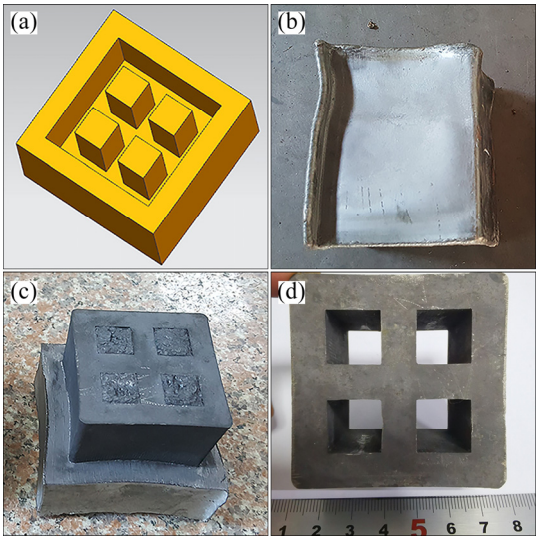

Fig. 1 Powder metallurgy Ti−45Al−7Nb−0.3W near net shape mold core model (a), HIPed specimen with steel package (b), photograph of specimen after removing package (c) and final near net shaped part (d)

The high temperature mechanical properties were carried out on a RRC−50 testing machine at the temperatures ranging from 20 to 1000 °C and initial strain rates of 1×10^{-3}, 1×10^{-4} and 5×10^{-5} s^{-1}, respectively. The specimens were cut from the HIPed part and the gauge section has dimensions of 8 mm × 3.4 mm × 3 mm. Before testing, all specimens were held at the test temperature for 30 min.

The phase constitution of the alloy analysis was carried out on a D/Max 2500 X-ray diffractometer (Cu K_α radiation, with voltage of 40 kV, current of 15 mA, diffraction angle (2θ) range of 10°−85° and step size of 0.02°). Quanta−200 scanning electron microscope (SEM) and Tecnai G220 Transmission electron microscope (TEM)

were used for microstructure analysis. The TEM foils were thinned by twin-jet electropolishing using a solution consisting of 6% perchloric acid, 34% butanol and 60% methanol at −28 °C and 25 V.

3 Results and discussion

3.1 Microstructure

The XRD pattern and SEM backscattered electron (BSE) image of the PM Ti−45Al−7Nb−0.3W alloy are presented in Fig. 2. The PM HIPed part is mainly composed of the γ phase and α_2 phase (Fig. 2(a)). The SEM image in Fig. 2(b) reveals that the microstructure of alloy shows a near γ microstructure, which is homogeneous and composed of equiaxed γ grains and a small amount of the α_2/γ lamellar colonies. The mean grain size of the γ phase is 9.3 μm. Meanwhile, the β phase whose fraction is too low to be detected by XRD is observed to distribute at the grain boundaries of γ phase and α_2/γ lamellar colonies with bright contrast in Fig. 2(b).

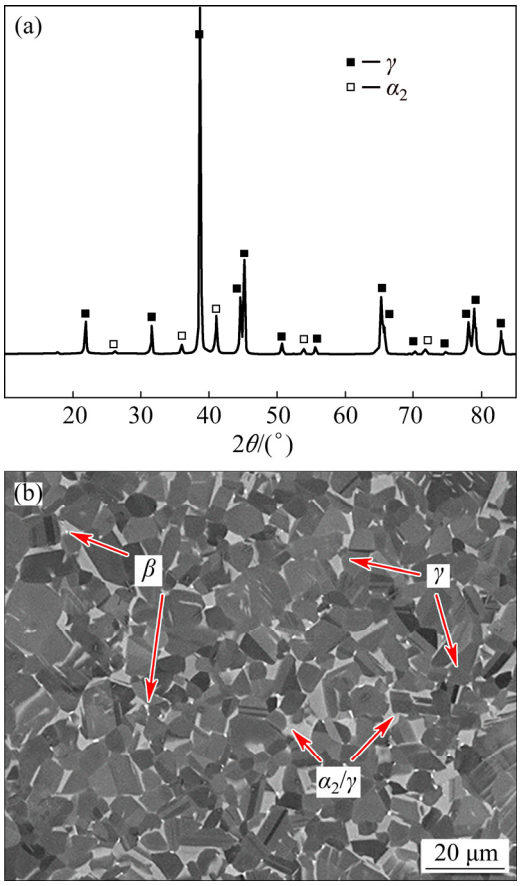

Fig. 2 XRD pattern (a) and SEM image (b) of HIPed Ti−45Al−7Nb−0.3W alloy

3.2 High-temperature mechanical properties

The influences of temperature on tensile properties of the PM Ti−45Al−7Nb−0.3W alloy with an initial strain rate of 1×10^{-4} s^{-1} are presented in Fig. 3(a). At room temperature, the ultimate tensile stress (UTS) and elongation of the alloy are 543 MPa and 0.2%, respectively. With increasing the temperature to 500 °C, the yield stress (YS) and ultimate tensile stress (UTS) decrease to 459 and 486 MPa, and the elongation is 1.4%. With further increasing temperature to 700 °C, the alloy exhibits peak YS (534 MPa) and UTS (575 MPa), which shows an anomalous strengthening. Then, the YS and UTS decrease again at elevated temperatures above 700 °C but the elongation always increases with temperature. When the TiAl alloy is tested at low temperatures (lower than 700 °C), the critical resolved shear stress (CRSS) to operate the ⟨011] superdislocation is lower than that of ordinary dislocation [22], the ⟨011] superdislocation can operate more easily. The dislocation motion is

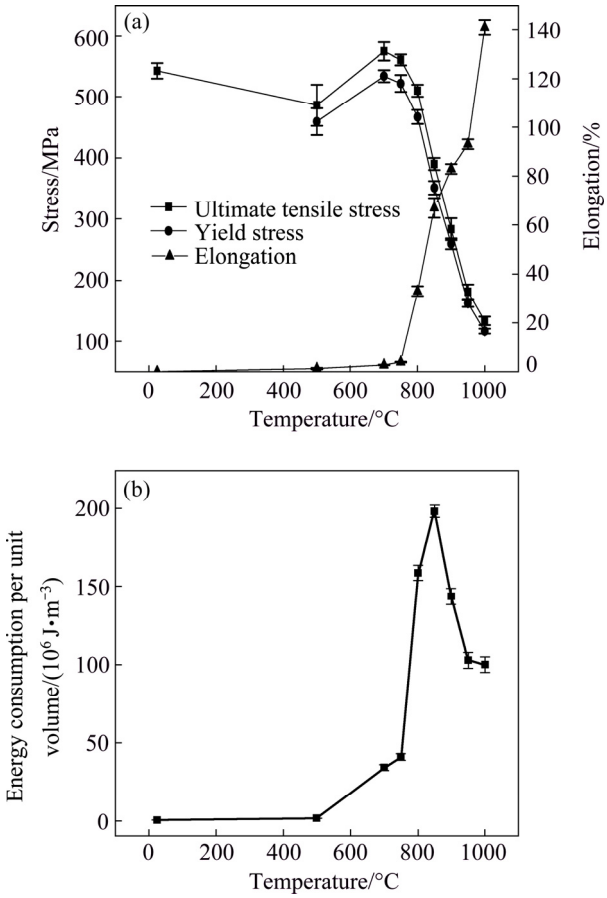

Fig. 3 Relationship between tensile properties and temperature of PM Ti−45Al−7Nb−0.3W alloy (a) and energy consumption per unit volume as function of temperature (b)

closely related to the cross-slip of 1/2⟨110] ordinary dislocations and ⟨011] superdislocations [23,24]. The cross-slip of the superdislocation can induce some planar defects such as superlattice intrinsic stack fault (SISF) and complex stacking fault (CSF) [25,26]. With the temperature increasing, the cross-slip of ordinary dislocation can be activated. The planar defects can pin on those ordinary dislocations, and result in the formation of Kear−Wilsdorf dislocation locks [27,28], which is wildly regarded as the reason for anomalous strengthening. Meanwhile, the elongation of the alloy is 4.1% at 750 °C, and rapidly increases to 33% at 800 °C, which indicates that the brittle-ductile transition temperature of the alloy is between 750 and 800 °C. At 1000 °C, the YS and UTS drop to 116 and 133 MPa, while the elongation increases to 141%, which shows the superplastic deformation characteristic of the alloy.

The comprehensive mechanical properties of alloy can be characterized by the energy consumption per unit volume when alloy fractures, which can be calculated by the area under engineering stress−strain curve, as Eq. (1).

$$v=\int_0^{\varepsilon}\sigma \mathrm{d}\varepsilon \tag{1}$$

where v is the energy consumption per unit volume when alloy fractures, σ is the engineering stress and ε is the engineering elongation during deformation. Figure 3(b) shows energy consumption per unit volume when alloy fractures as a function of the test temperature, which increases from 6.87×10^5 J/m^3 at 20 °C to 1.98×10^8 J/m^3 at 850 °C, and then decreases to 1×10^8 J/m^3 at 1000 °C. As a result, the alloy shows satisfactory comprehensive mechanical properties at 850 °C with the YS, UTS and elongation of 351 MPa, 390 MPa and 67%, respectively.

As already mentioned above, when the specimen is tested at 1000 °C with an initial strain rate of 1×10^{-4} s^{-1}, the elongation reaches 141%. This indicates that the alloy has superplastic deformation characteristic, and it is further confirmed by the tensile tests at 1000 °C with initial strain rates of 1×10^{-3} and 5×10^{-5} s^{-1}. The fractured specimens after deformation at 1000 °C with different initial strain rates and their engineering stress−strain curves are shown in Fig. 4. At 1000 °C, by decreasing the initial strain rate from 1×10^{-3} to 5×10^{-5} s^{-1}, the YS and UTS decrease from 195 and 230 MPa to 80 and 96 MPa, respectively, while the elongation increases from 85% to 303%. The superplastic elongation corresponds to high strain rate sensitivity coefficient (m), and the value of m is 0.3 in this study, which suggests that grain boundary sliding is the main deformation mechanism under this condition [29]. From the engineering stress−strain curves, it is found that the stress decreases obviously after it reaches the ultimate strength, indicating that the strain softening is dominant afterwards.

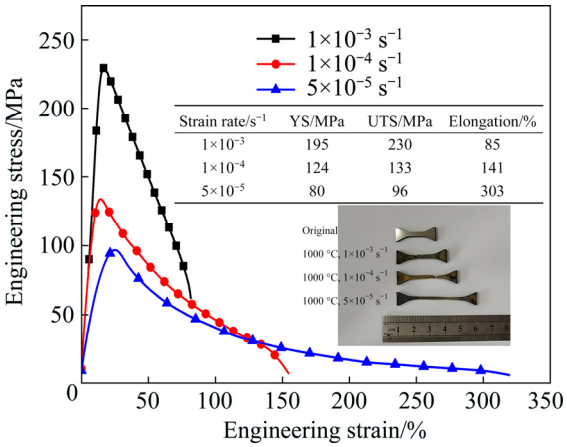

Fig. 4 Engineering stress−strain curves at 1000 °C with different initial strain rates and images of fractured specimens after tensile deformation

3.3 Microstructures after high-temperature tensile deformation

Figure 5 shows the fracture surfaces of the specimens tested at 20, 700, 850 and 1000 °C, respectively. It can be seen that the fracture modes are characterized by both the γ phase and the α_2/γ lamellar colonies. The specimens are found to exhibit a brittle fracture mode at the temperatures of 20 and 700 °C. Numerous cleavage planes shown in Fig. 5(a) indicate that the predominant mode at 20 °C is transgranular fracture. Translamellar cleavage along α_2/γ lamellar colonies was observed on the fracture surface of the specimen tested at 20 °C as shown in Fig. 5(a). At 700 °C, intergranular fracture along the γ grain boundaries is also observed in Fig. 5(b). This results from large deformation and imperfect lattice structure at grain boundaries, where microcracks are easy to be initiated and propagated due to the high stress concentration [19]. Many dimples can be clearly observed at 850 °C in Fig. 5(c), and the specimen exhibits a typical ductile fracture mode during

tensile, while the α_2/γ lamellar colonies show an interlamellar cleavage mode at 850 °C. With the tensile temperature increases to 1000 °C, dimples are deep (Fig. 5(d)), and this is consistent with the high elongation in tensile properties.

Figure 6 presents the SEM images of the deformed microstructures after tensile tests at 20, 700, 850 and 1000 °C, respectively. Compared with the microstructure of the HIPed specimen in Fig. 2(b), the microstructure after deformation at 20 and 700 °C shows no significant change and consists of equiaxed γ grains (Figs. 6(a) and (b)), and the α_2/γ lamellar structure shows no obvious orientation after being tested at 700 °C, as shown in Fig. 6(c). However, when the specimen is tested at 850 and 1000 °C, the γ grains are elongated along the load direction and a number of cavities are observed at grain boundaries (Figs. 6(d) and (e)).

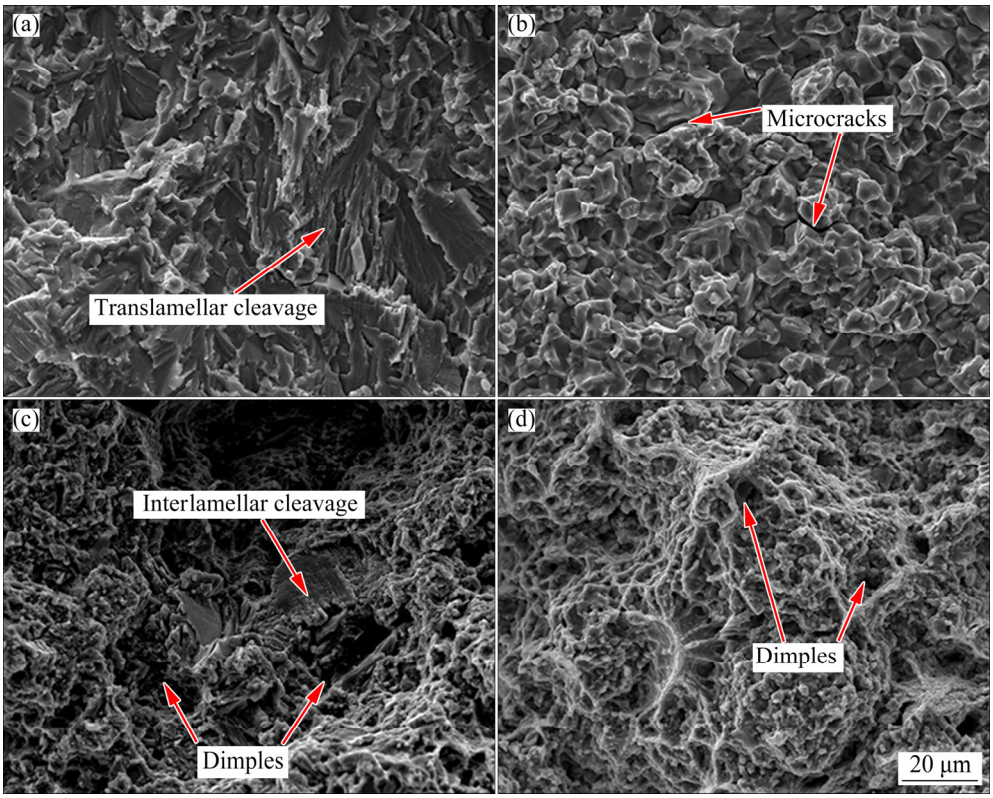

Fig. 5 Fracture surfaces of specimens tested at temperatures of 20 °C (a), 700 °C (b), 850 °C (c) and 1000 °C (d)

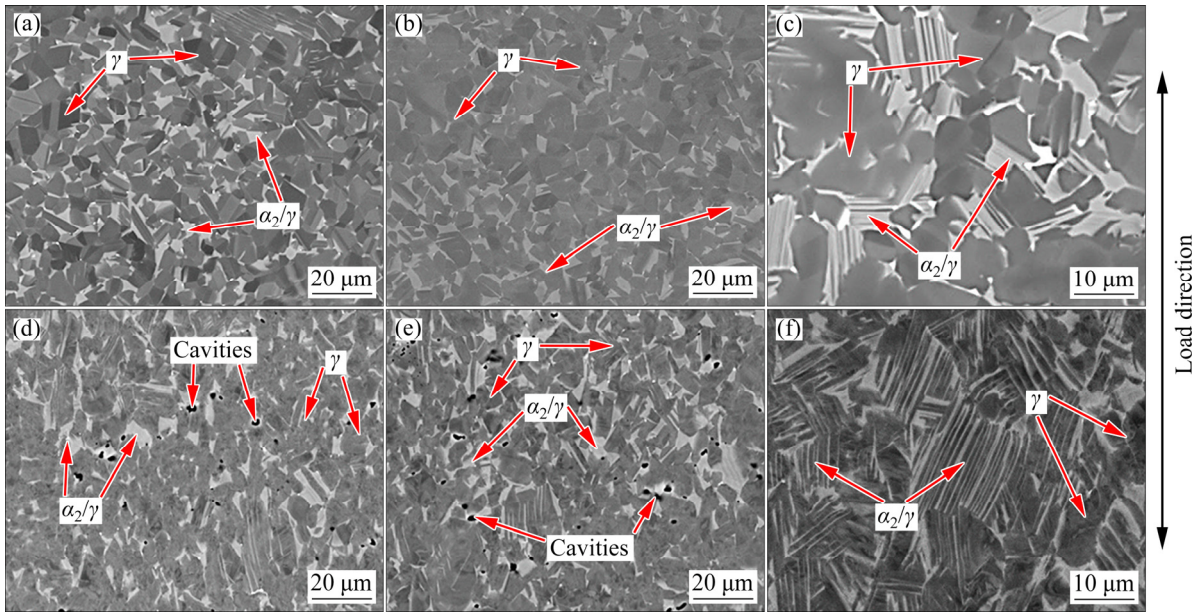

Fig. 6 SEM images of specimens tested at temperatures of 20 °C (a), 700 °C (b, c), 850 °C (d) and 1000 °C (e, f)

Especially after test at 1000 °C, α_2/γ lamellar colony is more aligned to the load direction (Fig. 6(f)).

The high-temperature deformation behaviors of HIPed TiAl alloy are mainly dependent on microstructure evolution of the γ grain at test temperature. Meanwhile, the coordination role of a few α_2/γ lamellar colonies cannot be ignored. Previous literature reported that the α_2/γ lamellar colonies have different orientations which lead to different deformability. The yield stress is low when the load direction lies close to the lamellar plane (soft orientation) and is high when the load direction is nearly normal to the lamellar plane (hard orientation) [30,31]. In this research, the lamellar plane shows no specific orientation after being tested at the temperature below 700 °C (Fig. 6(c)), the α_2/γ lamellar colonies in hard orientation could improve the flow stress of HIPed TiAl alloy [32]. However, due to the inhomogeneous deformation between the γ phase and α_2/γ lamellar colonies, large plastic deformation occurs at the grain boundaries which lead to the formation of the cavities. Large number of cavities would result in fracture during deformation. When tested at a high temperature, α_2/γ lamellar colonies are rotated and aligned to the load direction (Fig. 6(f)). The rotation of α_2/γ lamellar colonies can reduce the flow stress and is beneficial to the ductility of the alloy.

The bright-field TEM images of the HIPed and deformed specimens tested at 20 °C and 700 °C are shown in Fig. 7. As shown in Fig. 7(a), the microstructure of the HIPed specimen mainly consists of equiaxed γ grains. A low density of dislocation can be observed in the γ grains. Meanwhile, many annealing twins are observed to exist in HIPed microstructure. During HIP process, high stress and temperature provide distortion energy for grain growth and migration of high angle grain boundary, which facilitate the formation of twins. In addition, the stacking fault energy of TiAl is low [23], thus annealing twins are substantially formed in the HIPed microstructure. When the alloy is tensile tested at 20 °C, the mechanical twinning is observed in the microstructures (Fig. 7(b)) and the dislocation density is obviously higher than the as-HIPed alloy after being tensile deformed at 20 and 700 °C (Figs. 7(c) and (d)). Meanwhile, the dislocations in γ grain are arranged in cross type and tangled, which can lead to the rapid increment of stored energy after high temperature test.

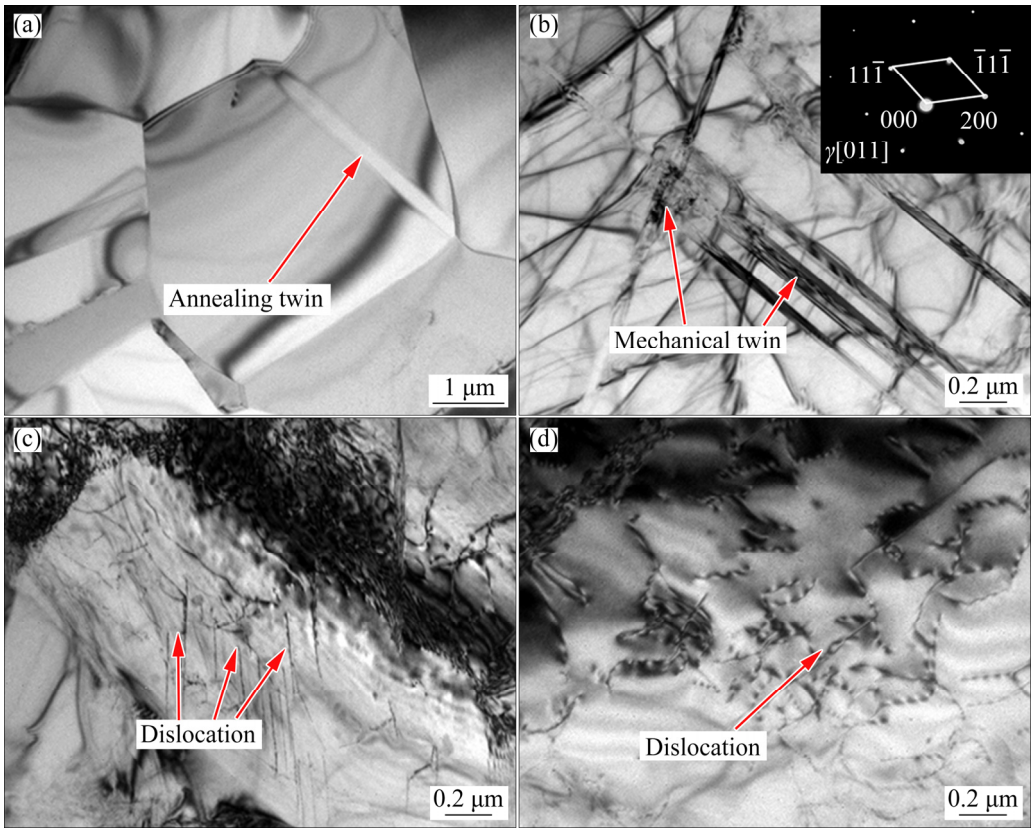

Fig. 7 TEM images of HIPed specimen (a) and specimen tested at temperatures of 20 °C (b, c) and 700 °C (d)

Figure 8 shows the TEM microstructure of the specimens deformed at 850 and 1000 °C. When the alloy tested at temperature above 850 °C, high density of dislocations tangled with each other in the γ grains (Fig. 8(a)). Meanwhile, dislocation networks are observed in γ grains (Fig. 8(b)). These dislocation networks formed related to entanglement of dislocations in γ grains while increasing the tensile temperature above 850 °C. COURET et al [33] reported that the dislocation networks can incorporate the dislocation, which is demonstrated by the presence of a number of extra half-threads in the rectangular network (Fig. 8(b)). The stable rectangular dislocation network consisting of cross-grid dislocations can impede the climbing and slipping of dislocation, and can result in severe work hardening [34,35]. With temperature increasing up to 1000 °C, high density of dislocations are observed accumulated at the grain boundaries due to dislocation climbing and slipping (Fig. 8(c)). These dislocations can cause large lattice distortion and improve the interface energy at grain boundary, which can improve the grain boundary migration. Therefore, grain boundary sliding (GBS) is the major mechanism for high-temperature deformation [36], which is activated by the interaction of dislocations, and deformation occurs along the most easily sliding surface. Due to the low stack fault energy of TiAl alloy [37−39], the mechanical twins are observed in TiAl alloys deformed at different temperatures (Fig. 7(b) and Fig. 8(d)). In the low stacking fault energy alloy, the mobility of dislocations reduces, so that twinning can be an alternative deformation mechanism to compensate the lack of glide systems [40,41]. Due to the fact that the twinning shear of mechanical twinning along 1/6⟨112]{111} is relatively small and atomic shuffling is not required during twinning, twins frequently appear in the γ grains and can contribute to relax stress concentration and accommodate deformation of the alloy [23].

When the specimen is tested at 1000 °C and 5×10^{-5} s^{-1}, the γ grains are more equiaxed (Fig. 9(a)) compared with those in the microstructure deformed at an initial strain rate of 1×10^{-4} s^{-1} (Fig. 6(e)). The density of dislocations decreases rapidly with decreasing the strain rate, and dislocations mainly appear at the grain boundaries (Fig. 9(b)). It can be seen from Fig. 4 that the ultimate tensile strength is closely related to the strain rate. With increasing the strain rate, the deformation resistance increases, and slipping of the dislocation is impeded. Therefore, dislocation accumulation occurs faster than recovery, resulting in a rapid increase in flow stress [42]. On the other

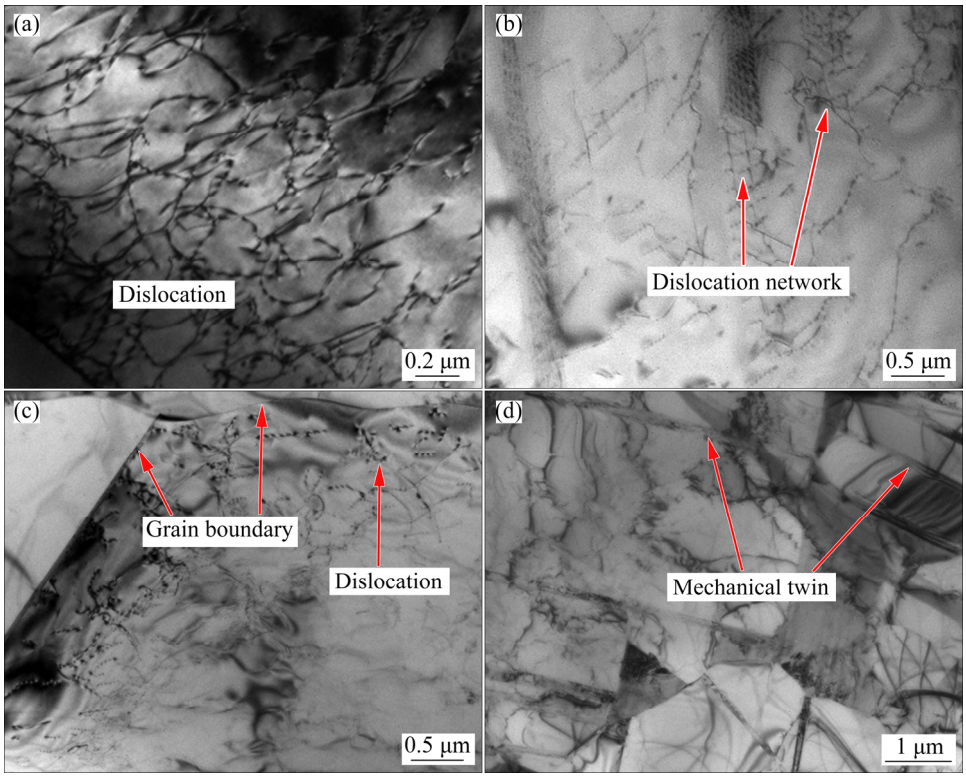

Fig. 8 TEM images of specimens tested at temperature of 850 °C (a, b) and 1000 °C (c, d)

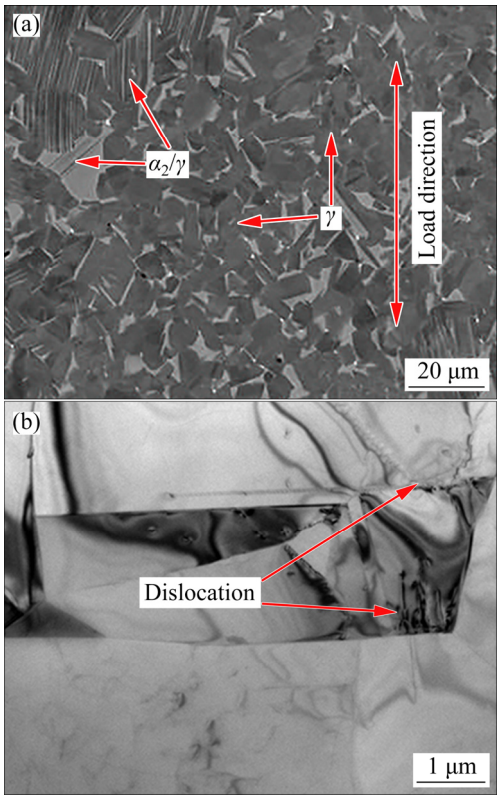

Fig. 9 SEM (a) and TEM (b) images of specimen tested under conditions of 1000 °C and 5×10^{-5} s^{-1}

hand, when the strain rate is high, deformation of the HIPed alloy is still mainly related to climbing and slipping of dislocation and twinning (Figs. 8(c) and (d)). Thus, grains are elongated along the load direction, and a number of caves are found at grain boundaries (Fig. 6(e)). With decreasing the strain rate, the deformation process is longer, which is beneficial for dislocation movement, and offers enough time for the recovery process to reduce the dislocation density (Fig. 9(b)) and release the stress concentration. Grain boundary sliding is the main deformation mechanism during superplastic deformation, and the movability of grain boundaries depends on the orientation of the neighboring grains. In the early stage of deformation, only the grain boundaries in a favorable orientation can slip more easily during high temperature deformation, while climbing and slipping of dislocation are still dominating the remaining grains because the original grains show no specific orientation. During the deformation process, slipping and climbing of the grain boundary dislocations can improve the slip ability of the grain boundaries, thus the γ grains start to rotate, and become equiaxed. Rotation of γ grains cannot contribute to deformability directly. However, as more γ grains rotate to the favorable orientation, grain boundary sliding and coordination mechanism of γ grains would be more easily activated. As a consequence, the flow stress is reduced and the elongation increases rapidly at low strain rates.

4 Conclusions

(1) The ultimate tensile strength of HIPed Ti−45Al−7Nb−0.3W part increases from 543 MPa at room temperature to 575 MPa at tensile temperature of 700 °C, and the elongation increases from 0.2% to 2.9%. The alloy shows satisfactory comprehensive mechanical properties at 850 °C with the YS, UTS and elongation of 351 MPa, 390 MPa and 67%, respectively.

(2) When the deformation temperature is lower than 700 °C, the deformation mechanism mainly refers to dislocation movements and mechanical twining in the near γ microstructure HIPed TiAl alloy. When the deformation temperature is higher than 850 °C, the deformation mechanism is related to the combination of dislocation movements, mechanical twinning, grain boundary sliding and the rotation of α_2/γ lamellar colonies.

(3) The near γ microstructure HIPed alloy displays superplastic characteristic at 1000 °C and strain rate of 5×10^{-5} s^{-1}. In this case, dynamic recovery reduces the dislocation density and the grain boundary sliding is promoted by γ grain rotation, which results in a rapid decrease in flow stress and improves elongation.

References

[1] ISMAEEL A, WANG Cun-shan. Effect of Nb additions on microstructure and properties of γ-TiAl based alloys fabricated by selective laser melting [J]. Transactions of Nonferrous Metals Society of China, 2019, 29: 1007−1016.

[2] LIANG Xiao-peng, LIU Yong, LI Hui-zhong, ZHOU Can-xu, XU Guo-fu. Constitutive relationship for high temperature deformation of powder metallurgy Ti−47Al−2Cr−2Nb−0.2W alloy [J]. Materials and Design, 2012, 37: 40−47.

[3] YANG Yong, FENG He-ping, WANG Qi, CHEN Rui-run, GUO Jing-jie, DING Hong-sheng, SU Yan-qing. Improvement of microstructure and mechanical properties of TiAl−Nb alloy by adding Fe element [J]. Transactions of Nonferrous Metals Society of China, 2020, 30: 1215−1324.

[4] SUN Hong-fei, LI Xue-wen, FANG Wen-bin. Microstructures of PM Ti−45Al−10Nb alloy fabricated by reactive sintering [J]. Transactions of Nonferrous Metals

Society of China, 2015, 25: 1454−1459.

[5] LI Wei, LI Ming, LIU Jie, YANG Yi, CAI Dao-sheng, WEI Qing-song, YAN Chun-ze, SHI Yu-sheng. Microstructures and mechanical properties of nano-WC reinforced Ti−44.5Al−5Nb−0.5W−0.5C−0.2B alloy prepared by hot isostatic pressing [J]. Journal of Alloys and Compounds, 2019, 770: 640−648.

[6] LI Wei, YANG Yi, LI Ming, LIU Jie, CAI Dao-sheng, WEI Qing-song, YAN Chun-ze, SHI Yu-sheng. Enhanced mechanical property with refined microstructure of a novel γ-TiAl/TiB2 metal matrix composite (MMC) processed via hot isostatic press [J]. Materials and Design, 2018, 141: 57−66.

[7] KONAK A, KULTUREL-KONAK S, SMITH A E, NETTLESHIP I. Estimation of shrinkage for net-shape using a neural net work approach [J]. Journal of Intelligent Manufacturing, 2003, 14(2): 219−228.

[8] WANG Gang, XU Lei, TIAN Yu-xing, ZHENG Zhuo, CUI Yu-yong, YANG Rui. Flow behavior and microstructure evolution of a P/M TiAl alloy during high temperature deformation [J]. Materials Science and Engineering A, 2011, 528: 6754−6763.

[9] QIU Chun-lei, WU Xin-hua. High cycle fatigue and fracture behaviour of a hot isostatically pressed nickel-based superalloy [J]. Philosophical Magazine, 2013, 94: 242−264.

[10] QIU Chun-lei, WU Xin-hua, MEI Jun-fa, ANDREWS P, VOICE W. Influence of heat treatment on microstructure and tensile behavior of a hot isostatically pressed nickel-based superalloy [J]. Journal of Alloys and Compounds, 2013, 578: 454−464.

[11] YUAN Wei-xing, MEI Jun-fa, SAMAROV V, SELIVERSTOV D, WU Xin-hua. Computer modelling and tooling design for near net shaped components using hot isostatic pressing [J]. Journal of Materials Processing Technology, 2007, 182: 39−49.

[12] HE Wei-wei, LIU Yong, TANG Hui-ping, LI Yun-ping, LIU Bin, LIANG Xiao-peng, XI Zheng-ping. Microstructural characteristics and densification behavior of high-Nb TiAl powder produced by plasma rotating electrode process [J]. Materials and Design, 2017, 132: 275−282.

[13] HABEL U, MCTIERNAN B J. HIP temperature and properties of a gas-atomized γ-titanium aluminide alloy [J]. Intermetallics, 2004, 12: 63−68.

[14] YANG Chao, HU Da-wei, WU Xin-hua, HUANG Ai-jun, DIXON M. Microstructures and tensile properties of hot isostatic pressed Ti4522XD powders [J]. Materials Science and Engineering A, 2012, 534: 268−276.

[15] SHAGIEV M R, SENKOV O N, SALISHCHEV G A, FROES F H. High temperature mechanical properties of a submicrocrystalline Ti−47Al−3Cr alloy produced by mechanical alloying and hot isostatic pressing [J]. Journal of Alloys and Compounds, 2000, 313: 201−208.

[16] CHENG Liang, CHANG Hui, TANG Bin, KOU Hong-chao, LI Jin-shan. Deformation and dynamic recrystallization behavior of a high Nb containing TiAl alloy [J]. Journal of Alloys and Compounds, 2013, 552: 363−369.

[17] KANANI M, HARTMAIER A, JANISCH R. Stacking fault based analysis of shear mechanisms at interfaces in lamellar TiAl alloys [J]. Acta Materialia, 2016, 106: 208−218.

[18] XU Mang, LIU Guo-hai, LI Tian-rui, WANG Bing-xing, WANG Zhao-dong. Microstructure characteristics of Ti−43Al alloy during twin-roll strip casting and heat treatment [J]. Transactions of Nonferrous Metals Society of China, 2019, 29: 1017−1025.

[19] LIU Yong, LIANG Xiao-peng, LIU Bin, HE Wei-wei, LI Jian-bo, GAN Zi-yang, HE Yue-hui. Investigations on processing powder metallurgical high-Nb TiAl alloy sheets [J]. Intermetallics, 2014, 55: 80−89.

[20] LI Hui-zhong, QI Ye-long, LIANG Xiao-peng, ZHU Ze-xiao, LV Feng, LIU Yong, YANG Yi. Microstructure and high temperature mechanical properties of powder metallurgical Ti−45Al−7Nb−0.3W alloy sheets [J]. Materials and Design, 2016, 106: 90−97.

[21] LI Hui-zhong, LONG Yu, LIANG Xiao-peng, CHE Yi-xuan, LIU Zhen-qi, LIU Yong, XU Hao, WANG Li. Effects of multiaxial forging on microstructure and high temperature mechanical properties of powder metallurgy Ti−45Al−7Nb−0.3W alloy [J]. Intermetallics, 2020, 116: 106647.

[22] MECKING H, HARTIG C H, KOCKS U F. Deformation modes in γ-TiAl as derived form the single crystal yield surface [J]. Acta Materialia, 1996, 44: 1309−1321.

[23] APPEL F, PAUL J D H, OEHRING M. Gamma titanium aluminide alloys: Science and technology [M]. Weinheim, Germany: Wiley-VCH, 2011.

[24] APPEL F, WAGNER R. Microstructure and deformation of two-phase γ-titanium aluminides [J]. Materials Science and Engineering R, 1998, 22: 187−268.

[25] ZUPAN M, HEMKER K J. Yielding behavior of aluminum-rich single crystalline γ-TiAl [J]. Acta Materialia, 2003, 51: 6277−6290.

[26] YUAN Yong, LIU Hong-wei, ZHAO Xiao-ning, MENG Xiang-kang, LIU Zhi-guo, BOLL T, AL-KASSAB T. Dissociation of super-dislocations and the stacking fault energy in TiAl based alloys with Nb-doping [J]. Physics Letters A, 2006, 358: 231−235.

[27] GREENBERG B A, ANTONOVA O V, VOLKOV A Y, IVANOV M A. The non-monotonic temperature dependence of yield stress in TiAl and CuAu alloys [J]. Intermetallics, 2000, 8: 845−853.

[28] CAILLARD D. Yield-stress anomalies and high-temperature mechanical properties of intermetallics and disordered alloys [J]. Materials Science and Engineering A, 2001, 10: 74−83.

[29] IMAYEV V M, GANEEV A A, IMAYEV R M. Principles of achieving superior superplastic properties in intermetallic alloys based on γ-TiAl+α_2-Ti_3Al [J]. Intermetallics, 2018, 101: 81−86.

[30] UMAKOSHI Y, NAKANO T, YAMANE T. The effect of orientation and lamellar structure on the plastic behavior of TiAl crystals [J]. Materials Science and Engineering A, 1992, 152: 81−88.

[31] LIANG Xiao-peng, LIU Yong, LI Hui-zhong, GAN Zi-yang, LIU Bin, HE Yue-hui. An investigation on microstructural and mechanical properties of powder metallurgical TiAl alloy during hot pack-rolling [J]. Materials Science and Engineering A, 2014, 619: 265−273.

[32] KIM Y W. Effects of microstructure on the deformation and fracture of γ-TiAl alloys [J]. Materials Science and Engineering A, 1995, 192−193: 519−533.

[33] COURET A, CALDERON H A, VEYSSIÈRE P. Intralamellar dislocation networks formed by glide in γ-TiAl I: The mechanism of formation [J]. Philosophical Magazine, 2003, 83: 1699−1718.
[34] CHEN Xiao-qun, HUANG Bo-yun, HE Yue-hui, QU Xuan-hui, OU Wen-pei, ZHOU Ke-chao. Study of deformation behaviour of TiAl-based alloy at high temperature [J]. Rear Metal Materials and Engineering, 1996, 25: 22−27.
[35] CHENG Liang, CHEN Yi, LI Jin-shan, BOUZY E. Superplastic deformation mechanism of a γ-TiAl alloy with coarse and bimodal grain structure [J]. Materials Letters, 2017, 194: 58−61.
[36] TANG Bin, ZHAO Feng-tong, CHU Yu-dong, KOU Hong-chao, LI Jin-shan. Hot workability and superplasticity of low-Al and high-Nb containing TiAl alloys [J]. Journal of Materials Science, 2017, 69: 2610−2614.
[37] NIU Hong-zhi, KONG Fan-tao, CHEN Yu-yong, YANG Fei. Microstructure characterization and tensile properties of β phase containing TiAl pancake [J]. Journal of Alloys and Compounds, 2011, 509: 10179−10184.
[38] WU Yu-lun, HU Rui, YANG Jie-ren, XUE Xiang-yi. High-temperature rotary-bending fatigue characteristics of a high Nb-containing beta-gamma TiAl alloy [J]. Materials Science and Engineering A, 2018, 735: 40−48.
[39] LI Hui-zhong, QI Ye-long, LIANG Xiao-peng, WANG Zi-jun, SANG Feng-jian, LIU Yong. Effects of pack rolling temperature on microstructure and mechanical properties of powder metallurgical Ti−45Al−7Nb−0.3W alloy [J]. Journal of Materials Science, 2017, 69: 1806−1811.
[40] LI Jian-bo, LIU Yong, LIU Bin, WANG Yan, CAO Peng, ZHOU Can-xu, XIANG Chun-jie. HE Yue-hui. High temperature deformation behavior of near γ-phase high Nb-containing TiAl alloy [J]. Intermetallics, 2014, 52: 49−56.
[41] OUYANG Si-hui, LIU Bin, LIU Yong, ZAN Xiang, LIANG Xiao-peng, LI Zheng. Dynamic tensile behavior of PM Ti−47Al−2Nb−2Cr−0.2W intermetallics at elevated temperatures [J]. Transactions of Nonferrous Metals Society of China, 2019, 29: 1252−1262.
[42] GONG Xue-bo, DUAN Zhen-xin, PEI Wen, CHEN Hua. Superplastic deformation mechanisms of superfine/nanocrystalline duplex PM-TiAl-based alloy [J]. Materials, 2017, 10: 1103.

粉末冶金热等静压方法制造的近净成形 Ti−45Al−7Nb−0.3W 合金的组织及高温力学性能

李慧中[1,2,3]，车逸轩[1]，梁霄鹏[1,2,3]，陶 慧[1]，张 强[1]，陈飞虎[1]，韩 硕[1]，刘 彬[2]

1. 中南大学 材料科学与工程学院，长沙 410083；
2. 中南大学 粉末冶金国家重点实验室，长沙 410083；
3. 中南大学 有色金属材料科学与工程教育部重点实验室，长沙 410083

摘 要：采用热等静压(HIP)方法制造近净成形的 Ti−45Al−7Nb−0.3W(摩尔分数，%)合金零件，并采用 X 射线衍射(XRD)、扫描电子显微镜(SEM)和透射电子显微镜(TEM)技术研究热等静压制备的 Ti−45Al−7Nb−0.3W 合金的显微组织和高温力学性能。结果表明，在 700 °C 条件下，热等静压制备的合金的屈服强度和极限抗拉强度分别为 534 和 575 MPa。该合金在 850 °C 时表现出良好的综合力学性能。在变形温度为 1000 °C、初始应变率为 5×10^{-5} s^{-1} 时合金表现出超塑性特性。当拉伸温度低于 750 °C 时主要变形机制为位错滑移和机械孪生。当变形温度高于 800 °C 时，位错在晶界堆积，促进晶界滑移和晶粒旋转。

关键词：TiAl 合金；近净成形；粉末冶金；高温力学性能

(Edited by Xiang-qun LI)